

A $FWHM - K_2$ correlation in Black-Hole transients

J. Casares

Instituto de Astrofísica de Canarias, 38205 La Laguna, S/C de Tenerife, Spain

Departamento de Astrofísica, Universidad de La Laguna, E-38206 La Laguna, S/C de Tenerife, Spain

ABSTRACT

We compare H_α emission profiles of 12 dynamically confirmed black holes (BHs) and 2 neutron star X-ray transients (SXTs) in quiescence with those of a sample of 43 Cataclysmic Variables (CVs), also quiescent. The full-width-half maximum ($FWHM$) of the H_α line in SXTs is tightly correlated with the velocity semi-amplitude of the donor star $K_2 = 0.233(13) FWHM$. This new correlation, when combined with orbital periods (i.e. through photometric light curves), opens the possibility to estimate compact object mass functions from single integration, low-resolution spectroscopy. On the other hand, CVs above the period gap are found to follow a flatter correlation, a likely consequence of their larger mass ratios. We also find that the $FWHM$ traces the disc velocity at $\approx 42\% R_{L1}$, independently of binary mass ratio. In addition, for a given $FWHM$, BHs tend to have lower EW s than CVs. This might be explained by the fact that CVs must be seen at higher inclinations to mimic the same projected disc velocities as BH SXTs. For the same reason CVs with $FWHM \gtrsim 1500 \text{ km s}^{-1}$ are mostly eclipsing while none of our sample BHs are. Further, we show that there is a vacant/unoccupied region for CVs in the $FWHM - EW$ plane defined by $FWHM > 2568 \sqrt{(1 - (9/EW)^2)}$ (km/s). Both the $FWHM - K_2$ correlation and the $FWHM - EW$ plane can be exploited, together with photometric light curves, to efficiently discover quiescent BHs in deep H_α surveys of the Galactic Plane.

Subject headings: accretion, accretion disks - binaries: close - Stars: black holes, neutron stars, dwarf novae, novae, cataclysmic variables - X-rays: stars

1. Introduction

Black holes (BH) provide unique laboratories to study key astrophysical phenomena such as accretion, the production of relativistic outflows and gamma ray bursts (e.g. Fender & Gallo 2014; Brown et al. 2000). BHs are usually discovered in transient X-ray binaries (SXTs) thanks to their dramatic, large-amplitude X-ray outbursts¹. These are caused by thermal-viscous instabilities in accretion discs which are (slowly) fed by matter transferred from a (donor) companion star (Lasota 2001). The distribution of BH masses and binary periods provide fundamental constraints to models of supernovae explosions and compact binary evo-

lution. Unfortunately, our understanding of the physics involved in these processes is still patchy because observational data are severely limited by small samples.

The current sample of ~ 50 BH SXTs, with only 17 dynamical confirmations, is the tip of the iceberg of a hidden population of hibernating BHs (see Casares & Jonker 2014). The size of the overall population is highly uncertain. Extrapolation of the number of SXTs discovered in the X-ray era suggests that several thousand dormant BHs are awaiting to be discovered (van den Heuvel 1992; Tanaka & Shibazaki 1996; Romani 1998). On the other hand, modern population-synthesis models predict an even larger population of $\sim 10^4 - 10^5$ SXTs (Pfahl et al. 2003; Yungelson et al. 2006). Observational constraints are likely biased low because they suffer from incompleteness and neglect

¹By contrast, persistent X-ray binaries tend to harbour neutron stars.

a hitherto unexpected population of long period SXTs with very long duty cycles or even suppressed outburst activity (cf. Ritter & King 2002; Menou et al. 1999). Furthermore, there is mounting evidence for the existence of a population of X-ray obscured or intrinsically faint BH SXTs (Corral-Santana et al. 2013; Armas Padilla et al. 2014). It has been shown that the latter could be members of a sizeable population of short period BH transients with low outburst luminosities (Maccarone & Patruno 2013). And finally, the recent discovery of the first Be/BH binary indicates that some BHs might be accreting "silently" from the slowly outflow winds of rapidly rotating Be-type stars (Casares et al. 2014). While binary population models predict a very modest number of Be/BH binaries in the Milky Way (Belczynski & Ziolkowski 2009; Grudzinska et al. 2015) empirical constraints, with only one detection yet, are very loose. Altogether, the only way to make significant progress in our knowledge of the Galactic population of BHs requires the discovery of a large sample of quiescent SXTs and this demands a new research methodology.

Quiescent BH SXTs are particularly difficult to find since they are relatively faint across the electromagnetic spectrum in this state. By their very nature, quiescent states are characterised by extremely low accretion levels ($< 10^{-9} M_{\odot} \text{ yr}^{-1}$). The inner disc is truncated in an advected flow and, further, the lack of a solid surface (an exclusive signature of BH) results in extremely weak X-ray, UV and radio luminosities (Narayan & McClintock 2008; Miller-Jones et al. 2011). On the other hand, the optical spectrum is dominated by the low-mass donor star, with superposed emission lines from the accretion disc gas. The lack of a hard radiation field implies that only emission from neutral H and He is detected. Crucially, the strongest emission line is H_{α} , but several other Galactic populations are also strong H_{α} emitters, such as Cataclysmic Variables (CVs), Symbiotic binaries, flare stars, reddened Be stars, T Tauri and other classes of young stellar objects. As a consequence, H_{α} surveys of the Galactic plane are vastly outnumbered by these populations of contaminating H_{α} emitters. Attempts to clear out the sample using color selection cuts (Corral-Santana et al. 2008) or X-ray diagnostics (Jonker et al. 2011) still have to prove their effectiveness. Inter-

estingly, new generation radio surveys (SKA and its pathfinders) may offer an alternative route to detect quiescent BHs given the increase in radio-to-X-ray flux ratios at very low luminosities (Maccarone 2005).

Here we present the discovery of a correlation between the width of the H_{α} line and the projected velocity of the companion star in quiescent SXTs. This property can be applied, in combination with photometric orbital periods, to gather compact object mass functions and flag new potential BHs. This strategy can be turned into a novel technique to unveil hibernating BHs, technique which appears much more efficient than traditional methods based on time-consuming spectroscopic monitoring of new X-ray novae.

2. The sample

2.1. X-ray Transients

We have assembled a spectroscopic database of dynamically confirmed BH SXTs with H_{α} emission (see Table 1). Most spectra were collected by us (V404 Cyg, BW Cir, N Mus 91, GS 2000+25, A0620-00, XTE J1650-500, XTE J1859+226, GRO J0422+320, XTE J1118+480) and have been presented in several publications, while others were kindly provided by J. Orosz (XTE J1550-564), R. Remillard (N Oph 77) and A. Filipenko (N. Vel 93). In addition, three new unpublished spectra of GRO J0422+320 were obtained on the night of 28 Jan 2009 with ALFOSC on the 2.5m Nordic Optical Telescope (NOT) at the Observatorio del Roque de los Muchachos. Integration time was set to 2400s and we used grism #4 and 1" slit to cover the range $\lambda\lambda 3820-9140$ at 360 km s^{-1} resolution. Seventy unpublished H_{α} spectra of V404 Cyg were also collected between 1994-2005 with the 2.5m Isaac Newton Telescope (INT) and the 4.2m William Herschel Telescope (WHT) at resolutions 36–134 km s^{-1} . Five additional spectra of V404 Cyg were obtained on the nights of 5 and 7-8 July 2008 at 200 km s^{-1} resolution with the 2.1m telescope at the Observatorio San Pedro Mártir (SPM). Finally the sample also includes spectra of the two only neutron star SXTs with a reported radial velocity curve of the companion star, Cen X-4 and XTE J2123-058. Table 1 provides the main observational details and associated references for every system.

2.2. Cataclysmic Variables

We also collected a database of H_α spectra of Cataclysmic Variables (CVs) in quiescence including 41 dwarf novae and two intermediate polars, also classified as classical novae (GK Per and DQ Her). Most of the spectra were acquired during several observing campaigns and Service nights performed with the WHT in 1992, 1993, 1998 and 2006, the INT in 1992, 2001, 2008 and 2009, the NOT telescope in 2008, 2009 and 2012, the 2.2m telescope at Calar Alto Observatory in 1995 and the 2.1m telescope at SPM in 2008. The WHT spectra were obtained with ISIS and the R1200R grating which delivers 40 km s^{-1} resolution at H_α . The INT spectra were obtained with the IDS spectrograph and gratings R150V, R300V, R900V and R1200R covering the H_α region at $50\text{--}320 \text{ km s}^{-1}$ resolution. For the NOT campaigns we used ALFOSC and grism #7 with different slit widths providing $235\text{--}310 \text{ km s}^{-1}$ resolution. The Calar Alto data were collected with the CASSPEC spectrograph, the f3 camera and grating #11 in second order which delivered 27 km s^{-1} resolution. The SPM spectra were obtained with the Boller & Chivens spectrograph and a 600 l/mm grating to yield 192 km s^{-1} resolution. Spectra of 13 CVs (BV Cen, EY Cyg, DX And, HS0218+3229, AH Her, HS2325+8205, SDSS J100658.40+233724, U Gem, CTCV J1300-3052, OY Car, V2051 Oph, SDSS 103533.02+055158 and SDSS J143317.78+101123.3) were kindly provided by different authors while H_α parameters for other 15 CVs were compiled from literature. In addition, spectra of WZ Sge were retrieved from the ING archive and reduced by us. The final collection of CV spectra were employed as a test sample for comparison with the H_α properties of SXTs. All the CVs have secured velocity amplitudes (K_2) of their companion stars either through radial velocity studies or eclipse light curve solutions (for short period binaries where the companion star is undetected). Table 2 summarizes the main observational details of the CV database. The database is intended to be a representative sample of quiescent CVs with available K_2 determinations although we warn about possible selection effects. These will be addressed in the following Section.

3. The $FWHM - K_2$ correlation

Full-width-half-maximum ($FWHM$) values were obtained from gaussian fits to individual H_α profiles in every SXT. The fitted model consists of a constant plus a Gaussian function. Continuum rectified spectra were fitted in a window of $\pm 10000 \text{ km s}^{-1}$, centered on the H_α line after masking the neighboring HeI line at $\lambda 6678$. We adopted $1\text{-}\sigma$ formal errors on the fitted parameter as derived through χ^2 minimization. Fig. 1 displays some fit examples to average line profiles covering the entire range of line widths displayed by our data. It is clear from the figure that a simple Gaussian does not provide an accurate description of very broad profiles with large double peak separations. However, we find that the $FWHM$ given by the Gaussian model is within 10% of other width parameters obtained from more sophisticated double-Gaussian models. And, more importantly, it is far more robust since double-Gaussian models can easily fail when fitting low signal-to-noise profiles. In addition to the $FWHM$, we also extracted equivalent widths (EW) by integrating the H_α flux in individual spectra, after continuum normalization.

Our 266 spectra of V404 Cyg span over 20 yr and, therefore, present the most complete database yet for the analysis of the secular evolution of accretion discs in quiescent BHs. Fig. 2 presents the evolution of both line parameters, $FWHM$ and EW , in V404 Cyg. The data points have been folded into 50 day bins, except for the first 30 days where 1 day bins were used to better trace the rapid evolution through the outburst. The plot shows a steep rise in $FWHM$ (drop in EW) followed by a plateau phase starting ~ 1300 days after the peak of the outburst. By taking the $FWHM$ as a proxy of the disc radius, Fig. 2 indicates that the accretion disc shrinks during outburst, recovering an equilibrium radius ~ 3.5 yr after the maximum. Evidence of accretion disc shrinkage following outburst has been reported for CVs using eclipse timing and eclipse mapping techniques (Smak 1984; Baptista & Catalán 2001). Because we are interested here in comparing average properties of stable quiescent discs in SXTs we decided to trim all data obtained within ~ 1300 days after the peak of the outburst. This leaves 127 useful spectra of V404 Cyg (all since 1993), 94

of BW Cir and 3 of GRO J0422+320 (from 2009).

Table 3 lists the mean $FWHM$ and EW values for SXTs, where the quoted uncertainties represent 1 standard deviation in the distribution of individual measurements. Therefore, our errors mostly reflect time variability in line width and normalized flux. Line variability is mainly caused by aperiodic flares (Hynes et al. 2002) or long-lived disc asymmetries (e.g. hot spots), modulated with the orbital period. In the cases of N. Oph 77 and Vel 93 only one phase averaged spectrum is available and, thus, we adopt $\sigma_{FWHM} = 0.1 FWHM$ to account for the average 10% variability displayed by the remaining binaries. By the same token, we adopt $\sigma_{EW} = 0.22 EW$ for objects where only one spectrum is available, based on the mean standard deviation in the EW s of the remaining systems. Instrumental resolution was subtracted quadratically from every $FWHM$ value and, therefore, the H_α widths quoted in Table 3 are intrinsic. Table 3 also provides fundamental binary parameters, chiefly the orbital period (P), the radial velocity semi-amplitude of the companion star (K_2) and the mass of the compact star (M_1) and inclination (i), when available, with their associated references.

We also collected $FWHM$ s and EW s from H_α lines in our sample of CV spectra listed in Table 2. In the case of 14 eclipsing binaries (EM Cyg, EX Dra, HS 2325+8205, DQ Her, SDSS J100658.40+233724.4, U Gem, IP Peg, CTCV J1300-3052, HT Cas, OY Car, V2051 Oph, SDSS 103533.02+055158.3, WZ Sge and SDSS J143317.78+101123.3) only spectra obtained ± 0.05 phases away from the eclipse minimum were considered. As already mentioned, $FWHM$ s and EW s values were obtained from the literature for 15 CVs. For these cases we adopt a 7% error in $FWHM$ and 14% error in EW , derived from the mean variability measured in the other 28 CVs. These values are listed in Table 4, together with determinations of the orbital period and K_2 velocities.

In Figure 3 we compare K_2 versus $FWHM$ and it can be seen that these quantities are tightly correlated in SXTs, with a Pearson correlation coefficient $r = 0.99$. A linear fit yields the following relation

$$K_2 = 0.233(13) FWHM \quad (1)$$

where both quantities are given in km s^{-1} . A second order polynomial fit is not justified since the constant coefficient is consistent with zero at 1σ . In order to assess the error in K_2 estimated from the correlation we computed the difference with the true (dynamical) K_2 for our 14 SXTs. The values are found to follow a Gaussian distribution with standard deviation of 22 km s^{-1} . We therefore conclude that robust estimates of the K_2 velocity can be obtained from the width of the H_α line in SXTs. The uncertainty in the coefficient of the correlation was estimated through a Monte-Carlo simulation of 10^4 events, assuming that the difference between the model and true K_2 values follow a Gaussian distribution with $\sigma = 22 \text{ km s}^{-1}$.

The $FWHM - K_2$ correlation is expected from basic equations. Assuming that $FWHM$ is determined by gas velocity at a characteristic disc radius R_W

$$\left(\frac{FWHM}{2}\right)^2 = \frac{GM_1}{R_W} \sin^2 i \quad (2)$$

where M_1 is the mass of the accreting star and i the binary inclination. On the other hand, the companion's velocity is given by

$$K_2^2 = \frac{GM_1^2}{a(M_1 + M_2)} \sin^2 i \quad (3)$$

with M_2 the mass of the companion star. Therefore,

$$\left(\frac{K_2}{FWHM}\right)^2 = \frac{R_W}{4a(1+q)} \quad (4)$$

where $q = M_2/M_1$ is the mass ratio and a the binary separation. If we now assume $R_W = \alpha R_{L1}$ (with $\alpha < 1$) and use Eggleton's relation (Eggleton 1983) to remove R_{L1}/a then

$$\frac{K_2}{FWHM} = \frac{\sqrt{\alpha f(q)}}{2} \quad (5)$$

where

$$f(q) = \frac{0.49(1+q)^{-1}}{0.6 + q^{2/3} \ln(1+q^{-1/3})} \quad (6)$$

In the domain of SXTs, with $q \simeq 0.05 - 0.15$, the dependence of Eq. 5 with q is modest because

$\sqrt{f(q)}$ varies between 0.77–0.69. For typical BH SXTs, with $q = 0.1$, $K_2/FWHM = 0.36\sqrt{\alpha}$ and hence, the empirical correlation, described by eq. 1, implies that the $FWHM$ of the H_α line in BH SXTs traces the disc velocity at about 41% R_{L1} . And given that $\sim 80\%$ of the line flux is contained within one $FWHM$ and that typical quiescent disc radii reach $\sim 0.5 - 0.6R_{L1}$ (Marsh et al. 1994; Casares et al. 1995b) we observe that the bulk of the H_α emission arises from the outermost regions of the accretion disc.

Equation 1 stems from the fact that the Keplerian velocity field in the H_α disc provides a fundamental dimension scale of the binary. Similarly to the rotational broadening of the donor star $V \sin i$ (see Wade & Horne 1988), the *mean* accretion disc velocity (traced by the $FWHM$) scales with the donor star’s velocity. Since both are projected velocities along the line of sight, the dependence on inclination cancels out. However, unlike $V \sin i$, this new correlation is only weakly dependent on binary mass ratio and hence results in a very tight linear regression. We also note that eq. 1 is more robust than a former empirical relation between K_2 and the double peak separation (Orosz et al. 1994; Orosz & Bailyn 1995) because the latter traces the tidal (outer disc) radius which can be strongly affected by disc asymmetries, the presence of S-wave distortions driven by hot-spots and anomalously low (sub-Keplerian) velocities (e.g. North et al. (2002)).

At this point it is instructive to compare how the CVs distribute in the $FWHM - K_2$ plane. But prior to this it is important to assess the impact of possible selection effects. To start with, since the companion star is mostly detected above the period gap, our reference sample is, in principle, biased toward large mass ratios. The effect is further exacerbated by the fact that the CV population in the 3-4 h period range is dominated by SW Sex and Novalike stars, systems in permanent outburst (Rodríguez-Gil et al. 2007). This explains the paucity of CVs with periods < 0.17 d in our list. To compensate for the deficit of binaries with small q values we made an effort to incorporate short period CVs. These are, however, strongly skewed towards high inclinations because only eclipsing CVs can yield reliable K_2 values (through light curve modeling) when the companion star is not detected. Fig. 4 presents his-

tograms of the distribution of orbital periods, mass ratios and inclinations in our CV sample, clearly depicting these selection effects. Mass ratios and inclination values were compiled from the references listed in Table 4 and Ritter & Kolb (2003). In the figure we make a distinction between CVs above and below/within the period gap.

Figure 4 shows that the distribution of mass ratios is clearly bimodal and can be described by two Gaussians: 32 long-period CVs cluster at $q = 0.63$ with $\sigma = 0.2$ while 11 short-period CVs define a much narrow peak centered at $q = 0.12$ and with $\sigma = 0.07$. We note that this is overall similar to the distribution of mass ratios obtained from the entire CV data available in the Ritter’s catalogue (Ritter & Kolb 2003). The figure also highlights the fact that our short period CVs are strongly biased toward high inclinations. By contrast, there seems to be no significant bias in the inclination of CVs above the gap. In view of this, we find justified to distinguish hereafter between short-period CVs (i.e. below/within the gap) and long-period CVs (above the gap), with the latter not being strongly affected by selection effects.

The bottom panel in Fig. 3 presents the location of the CVs in the $FWHM - K_2$ plane. The figure shows that long-period CVs display a similar regression to that found for SXTs albeit flatter, i.e. for a given K_2 , H_α lines are systematically broader than in SXTs. A linear fit yields $K_2 = 0.169(16) FWHM$, relation which could be used to infer K_2 velocities for quiescent CVs above the period gap. We attribute the flatter slope of the CV correlation to their comparatively larger mass ratios, which leads to smaller R_{L1} and thus smaller disc radii (in binary separation units).

If we now bring $q=0.63$ (i.e. the peak in the q distribution of long-period CVs) into eqs. 5-6 and set $K_2/FWHM = 0.169$ from the empirical fit one obtains $\alpha = 0.43$, in excellent agreement with what was found for SXTs. This implies that the $FWHM$ of the H_α line is always formed at about 42% R_{L1} , irrespectively of the binary mass ratio. Despite the large spread in mass ratios the CV correlation appears quite narrow, a consequence of the very weak dependence of $K_2/FWHM$ with q for large q values (see dotted lines in the bottom panel of Fig. 3).

The group of short-period CVs, on the other hand, concentrate at large $FWHM$ values be-

cause of their high inclinations. They are seen to depart from the trend defined by the long-period CVs, approaching the SXT correlation, a result of their small q -values. Although the short-period CVs represent a very biased sample, they are of particular interest because they define the upper limit in the $FWHM$ distribution of the CV population.

4. The $EW - FWHM$ plane

In a given system, the $FWHM$ of any emission line depends on the binary inclination, orbital period and the mass of the compact object. By bringing $K_2 = (2\pi a \sin i)/P(1+q)$ into eq. 5 and using Kepler's Third Law we find

$$FWHM \propto \frac{\sin i}{\sqrt{\alpha(1+q)^{4/3} f(q)}} \left(\frac{M_1}{P}\right)^{1/3} \quad (7)$$

Here, the dependence on mass ratio is extremely weak, with $\sqrt{(1+q)^{4/3} f(q)}$ varying in the range 0.80 to 0.69 for $q = 0.05 - 1$. Therefore, we can safely assume

$$FWHM \simeq A \left(\frac{M_1}{P}\right)^{1/3} \sin i \quad (8)$$

where A is a constant that can be calibrated using P and $FWHM$ values listed in Table 3, together with dynamical masses and inclinations available in the literature for 9 SXTs (also listed in Table 3). These yield a mean value $A = 876 \pm 48 \text{ km s}^{-1}$, when M_1 and P are expressed in units of M_\odot and days, respectively.

On the other hand, the EW of the H_α line depends on the binary geometry. For instance, Warner (1986) showed that the EW of H_β in CVs increases with inclination because of the reduction of continuum brightness as the disc is seen at large inclinations. Therefore, to a first-order approximation one can assume

$$EW \approx \frac{B}{\cos i} \quad (9)$$

where the constant $B = 9 \pm 8 \text{ \AA}$ has been calibrated using the distribution of EW s and inclinations listed in Table 3².

²If we use instead reliable masses and inclinations reported

Fig. 5 displays our sample of SXTs and CVs in the $EW - FWHM$ plane. Here we have used open triangles to mark eclipsing CVs. BHs are a factor ~ 10 more massive than white dwarfs or NS and thus should possess, on average, wider H_α lines by a factor ~ 2.2 . Instead, we observe that only one BH (XTE J1118+480) stands out clearly in the right side of the diagram with $FWHM > 2500 \text{ km s}^{-1}$. The remaining BHs are mixed up with CVs at lower $FWHM$ values because they either have long orbital periods (i.e. cases of V404 Cyg and BW Cir with $FWHM \sim 1000 \text{ km s}^{-1}$) or are viewed at lower inclinations. Fortunately, they cluster in the central part of the diagram between $FWHM \sim 1500 - 2500 \text{ km s}^{-1}$, a region populated by eclipsing CVs. Since the latter are easily detected through deep ($\sim 2-3$ mag) eclipses we conclude that non-eclipsing binaries with $FWHM \gtrsim 1500 \text{ km s}^{-1}$ are good candidates to host BHs. Incidentally, a population of (short-period) eclipsing BHs with very wide H_α lines would be expected in the right part of the diagram. Scaling from the eclipsing CVs we predict them to show a factor ~ 2.2 larger widths i.e. $FWHM \sim 4200 \text{ km s}^{-1}$. As a matter of fact, the transient X-ray binary Swift J1357-0933 has been proposed as an extreme inclination BH, although no dynamical solution is yet available (Corral-Santana et al. 2013). We have recently obtained 4 H_α spectra of Swift J1357-0933 with OSIRIS and the R300R grism on the 10.4m Gran Telescopio Canarias (GTC) on 29-30 June 2013, from which we measure $FWHM = 4085 \pm 328 \text{ km s}^{-1}$ and $EW = 131.9 \pm 14.5$. These values are indeed consistent with a short period BH seen at very high inclination. The position of Swift J1357.2-0933 is indicated by an asterisk in the diagram.

Using eqs. 8-9 one can define regions of constant M_1/P and inclination in the $EW - FWHM$ plane. These are marked in the bottom panel of Fig. 5 using dashed and dotted lines respectively. We stress, however, that the quoted inclinations must be considered as mere indicative given the crude approximation involved in eq. 9. The figure suggests (with all the caveats associated to low number statistics) that, for a given $FWHM$, BHs

in literature for a subset of 25 CVs from our Table 4 we find $A = 897 \pm 46 \text{ km s}^{-1}$ and $B = 7 \pm 5 \text{ \AA}$, in good agreement with the calibration obtained using SXTs.

tend to have lower EW s than CVs. This could be explained because, due to their shallower potential wells, CVs must be seen at higher inclinations to mimic the same projected disc velocities as BHs and, therefore, their H_α fluxes are less diluted by the accretion disc continuum. It is interesting to note the position of GRO J0422+320 in the upper left side of the diagram. While the mass of its BH is quite uncertain (see Casares & Jonker 2014) both the large EW and low M_1/P factor suggest it hosts a low-mass BH, in line with the results of Casares et al. (1995a) and Gelino & Harrison (2003).

Finally, we can tentatively define a forbidden region for CVs in the $FWHM - EW$ plane by taking extreme parameters i.e. $M_1 > 1.4 M_\odot$ and $P < 80$ min, the period minimum spike observed in the distribution of CV periods (Gänsicke et al. 2009). This yields $M_1/P > 25.2 M_\odot/d$ and thus $FWHM > 2568\sqrt{(1 - (9/EW)^2)}$, limit which is marked by a green solid line in the plot. As a test we have examined a random sample of 236 dwarf novae selected from Sloan DR7. Sloan CVs show the same trend as seen in Fig. 5 i.e. they populate the region leftwards of the green line, with a large spread towards high EW s up to $\sim 350 \text{ \AA}$.

5. Discussion: new strategies to detect dormant BHs

To make progress in our understanding of the formation and evolution of Galactic BHs it is essential to discover a large sample of secured (dynamically confirmed) BHs. This new sample would allow us to constrain the number density, the orbital period distribution and, ultimately, the BH mass spectrum. Only then we will be able to address fundamental questions such as the role of supernova models in shaping the distribution of BH masses, a current hot topic in the community (Özel et al. 2010; Farr et al. 2011; Kreidberg et al. 2012; Belczynski et al. 2012). Deep H_α surveys of the Galactic plane, combined with spectroscopic surveys, can efficiently select samples of H_α emitting objects with $FWHM > 1000 \text{ km s}^{-1}$. This width cut would allow instant removal of Galactic populations of narrow H_α emitters such as planetary nebulae, Be, chromospheric stars, T Tauri and other YSOs. Only high inclination CVs, due to the large gravitational fields of their accreting

white dwarfs, are able to produce wide H_α lines.

Fortunately, as we have shown, the width of the H_α line in quiescent BH and NS SXTs is tightly correlated with the projected velocity of the donor star. The $FWHM - K_2$ relation can, therefore, be exploited, together with supplementary information on orbital periods (e.g. from light curve variability), to gather "preliminary" mass functions (PMF) of compact objects from single epoch spectroscopy i.e. $PMF = 1.3 \times 10^{-9} P (FWHM)^3$, where P is given in days and $FWHM$ in km s^{-1} . K_2 values can be estimated from single integrations rather than expensive time resolved spectroscopy, allowing a search for dynamical BHs in much deeper fields and using a factor ~ 4 lower spectral resolution than usually employed. Therefore, the novel strategy that we propose is clearly much more efficient than standard spectroscopic techniques, aiming at measuring the orbit of the donor star from the Doppler shift of weak absorption lines. And it may be the only way to infer mass functions in extremely faint BH SXTs i.e. the bulk of the Galactic population. We also note that our technique can be easily executed in crowded regions like globular clusters, where HST time-series photometry can yield orbital periods while ground-based spectroscopy is severely limited by seeing conditions.

Fig. 6 demonstrates how BHs are nicely segregated from CVs and NS using the $FWHM - K_2$ correlation. Every BH (except GRO J0422+320) is located in the right hand part of the diagram, beyond the dotted vertical line. Therefore, targets with $PMF > 2 M_\odot$ are strong candidates to host BHs. It should be noted that the plotted CV $PMFs$ are, in most cases, robust upper limits to true mass functions because, by adopting eq. 1 we overestimate their real K_2 values. By comparing the PMF values with the true (dynamical) mass function of BHs one can estimate the typical uncertainty introduced by the $FWHM - K_2$ correlation. Relative errors in mass function are found to follow an approximate Gaussian distribution with $\sigma = 0.08$. Therefore, the $FWHM - K_2$ correlation allows us to estimate mass functions with typically $\sim 10\%$ uncertainty. As an example, we have applied eq. 1 to Swift J1357.2-0933, where our quiescent GTC spectra yield $FWHM = 4085 \pm 328 \text{ km s}^{-1}$. Extrapolating from eq. 1 we predict $K_2 = 952 \pm 93 \text{ km s}^{-1}$

which, when combined with $P = 0.117 \pm 0.013$ d, (Corral-Santana et al. 2013) leads to a record mass function $PMF = 10.5 \pm 3.3 M_{\odot}$. We note that this figure might even be slightly underestimated since the GTC spectra were taken only ~ 900 d. after the peak of the outburst (see Sect. 3). In any case, the effect would be small compared to our errorbar, which is dominated by propagating the large $FWHM$ uncertainty (driven by line variability) into the $FWHM - K_2$ relation and the mass function equation.

A big step forward in the exploitation of the $FWHM - K_2$ relation will likely come from the use of imaging techniques. Accurate H_{α} widths can be measured directly through a combination of customized narrow-band filters, removing the need for any spectroscopy at all. This brings in a new observational signature that we coin here *Photometric Mass Function* (PMF , taking advantage from the same acronym before). $PMFs$ open a novel concept, i.e. that of weighting mass functions photometrically, and lay the ground for the efficient discovery of new hibernating BHs in large survey volumes. We are currently working on this strategy.

Finally, it should be borne in mind that there is a strong selection effect against detecting high inclination BHs in X-ray selected samples. This is because flared accretion discs obscure X-rays and indeed none of the currently known dynamical BHs has an inclination $> 75^{\circ}$ (Narayan & McClintock 2005). Since a PMF -based sample will be selected by H_{α} widths and not X-ray emission we expect this strategy will uncover a significant number of high inclination and even eclipsing BHs. These hold the prospect to render the most accurate BH masses yet because the relative uncertainty in the inclination dominates the mass error budget. Clearly, the newly discovered BHs will have an strategic impact in the construction of the BH mass spectrum.

We would like to thank the anonymous referee for the valuable comments which helped to improve the quality of the paper. We also acknowledge the hospitality of the Department of Astrophysics of the Oxford University (UK) where part of this work was carried out. We are grateful to R. Remillard, A. Filippenko and J. Orosz for providing us with spectra of N. Oph 77, N. Vel 93 and

XTE J1550-564 respectively. Also to C. Watson, A. Bruch, K. Horne, C. Savoury, D. Steeghs, C. Copperwheat and S. Tulloch for the spectra of BV Cen, DX And, AH Her, CTCV J1300-3052, V2051 Oph, OY Car and SDSS J143317.78+101123.3, respectively. P. Rodríguez-Gil kindly provided spectra of HS0218+3229 and HS2325+8205 while J. Southworth those of SDSS J100658.40+233724 and SDSS 103533.02+055158.3. A selection of U Gem and EY Cyg spectra, the latest corrected for nebular emission, was provided by J. Echevarría. We thank R. Cornelisse for taking the GTC spectra of Swift J1357-0933. We are indebted to C. Zurita for conducting the San Pedro Mártir observations and also to the team of IAC Support Astronomers for obtaining CV spectra during Service time over several years. This paper makes use of data obtained from the Isaac Newton Group Archive which is maintained as part of the CASU Astronomical Data Centre at the Institute of Astronomy, Cambridge. This work is supported by DGI of the Spanish Ministerio de Educación, Cultura y Deporte under grants AYA2010-18080, AYA2013-42627 and SEV-2011-0187. Partially based on observations made with the GTC operated on the island of La Palma by the Instituto de Astrofísica de Canarias in the Spanish Observatorio del Roque de Los Muchachos of the Instituto de Astrofísica de Canarias.

REFERENCES

- Armas Padilla, M., Wijnands, R., Degenaar, N., Muñoz-Darias, T., Casares, J. & Fender, R.P. 2014, MNRAS, 444, 902
- Baptista, R., Catalán, M.S., Horne, K. & Zilli, D. 1998, MNRAS, 300, 233
- Baptista, R., Catalán, M.S. & Costa, L. 2000, MNRAS, 316, 529
- Baptista, R. & Catalán, M.S., 2001, MNRAS, 324, 599
- Baptista, R., Borges, B.W., Bond, H.E., Jablonski, F., Steiner, J.E. & Grauer, A.D., 2003 MNRAS, 345, 889
- Barrera, L.H. & Vogt, N., 1989 A&A, 220, 99
- Beekman, G., Somers, M., Naylor, T. & Hellier, C. 2000, MNRAS, 318, 9

- Belczynski, K. & Ziolkowski, J. 2009, *ApJ*, 707, 870
- Belczynski, K., Wiktorowicz, G., Fryer, C.L., Holz, D.E. & Kalogera, V. 2012, *ApJ*, 757, 91
- Billington, I., Marsh, T.R. & Dhillon, V.S. 1996, *MNRAS*, 278, 673
- Borges, B.W., Baptista, R., Papadimitriou, C. & Giannakis, O. 2008, *A&A*, 480, 481
- Brown, G.E., Lee, C.-H., Wijers, R.A.M.J., Lee, H.K., Israelian, G. & Bethe, H.A. 2000, *NewA*, 5, 191
- Bruch, A. 2003, *A&A*, 409, 647
- Bruch, A., Vriellmann, S., Hessman, F.V., Kochsiek, A. & Schimpke, T. 1997, *A&A*, 327, 1107
- Cantrell, A.G. et al. 2010, *ApJ*, 710, 1127
- Casares, J. 1996, *Astrophysics and Space Science Library*, Proc. of the 158th coll. of IAU, A. Evans and Janet H. Wood ed., Dordrecht: Kluwer Academic Publishers, 208, p.395
- Casares, J., Charles, P.A., Jones, D.H.P., Rutten, R.G.M. & Callanan, P.J. 1991, *MNRAS*, 250, 712
- Casares, J. & Charles, P.A. 1992a, *MNRAS*, 255, 7
- Casares, J., Charles, P.A. & Naylor, T. 1992b, *Nature*, 355, 614
- Casares, J., Charles, P.A., Naylor, T. & Pavlenko, E.P. 1993, *MNRAS*, 265, 834
- Casares, J. & Charles, P.A. 1994, *MNRAS*, 271, L5
- Casares, J., Martín, A.C., Charles, P.A., Martín, E.L., Rebolo, R., Harlaftis, E.T. & Castro-Tirado, A.J. 1995a, *MNRAS*, 276, L35
- Casares, J. Charles, P.A & Marsh, T.R. 1995b, *MNRAS*, 277, L45
- Casares, J., Martín, E.L., Charles, P.A., Molaro, P. & Rebolo, R. 1997, *NewA*, 1, 299
- Casares, J., Dubus G., Shahbaz, T., Zurita, C. & Charles, P.A. 2002, *MNRAS*, 329, 29
- Casares, J., Zurita C., Shahbaz, T., Charles, P.A. & Fender, R.P. 2004, *ApJ*, 613, L133
- Casares, J., Bonifacio, P., González Hernández, J.I., Molaro, P. & Zoccali, M. 2007, *A&A*, 470, 1033
- Casares, J. et al. 2009a, *ApJS*, 181, 238
- Casares, J., Martínez-Pais, I.G. & Rodríguez-Gil, P. 2009b, *MNRAS*, 399, 1534
- Casares, J. & Jonker, P.G. 2014, *SSRv*, 183, 223
- Casares, J., Negueruela, I., Ribó, M., Ribas, I., Paredes, J.M., Herrero, A. & Simón-Díaz, S. 2014, *Nature*, 505, 378
- Copperwheat, C.M., Marsh, T.R., Dhillon, V.S., Littlefair, S.P., Hickman, R., Gänsicke, B.T. & Southworth, J. 2010, *MNRAS*, 402, 1824
- Copperwheat, C.M. et al. 2012, *MNRAS*, 421, 149
- Corral-Santana, J.M., Casares, J., Martínez-Pais, I.G. & Rodríguez-Gil, P. 2008, *AIPC*, 1010, 79
- Corral-Santana, J.M., Casares, J., Shahbaz, T., Zurita, C., Martínez-Pais, I.G. & Rodríguez-Gil, P. 2011, *MNRAS*, 413, L15
- Corral-Santana, J.M., Casares, J., Muñoz-Darias, T., Rodríguez-Gil, P., Shabaz, T., Zurita, C., Torres, M.A.P. & Tyndall, A. 2013, *Science*, 339, 1048
- Davey, S. & Smith, R.C. 1992, *MNRAS*, 257, 476
- D'avanzo, P., Campana, S., Casares, J., Israel, G.L., Covino, S., Charles, P.A. & Stella, L. 2005, *A&A*, 444, 905
- Drew, J.E., Jones, D.H.P. & Woods, J.A. 1993, *MNRAS*, 260, 803
- Echevarría, J., Michel, R., Costero, R. & Zharikov, S. 2007, *A&A*, 462, 1069
- Eggleton, P.P. 1983, *ApJ*, 268, 368
- Farr, W.M., Sravan, N., Cantrell, A., Kreidberg, L., Bailyn, C.D., Mandel, I. & Kalogera, V. 2011, *ApJ*, 741, 103
- Fender, R. & Gallo, E. 2014, *SSRv*, 183, 323

- Filippenko, A.V., Leonard, D.C., Matheson, T., Li, W., Moran, E.C. & Riess, A.G. 1999, *PASP*, 111, 969
- Friend, M.T., Martin, J.S., Connon Smith, R. & Jones, D.H.P. 1990, *MNRAS*, 246, 637
- Gänsicke, B.T. et al. 2009, *MNRAS*, 397, 2170
- Gelino, D.M., Harrison, T.E. & McNamara, B.J. 2001, *AJ*, 122, 971
- Gelino, D.M. & Harrison, T.E. 2003, *ApJ*, 599, 1254
- Gilliland, R. L. 1982, *ApJ*, 263, 302
- Gonzalez Hernandez, J.I. & Casares, J. 2010, *A&A*, 516, A58
- Gonzalez Hernandez, J.I., Casares, J., Rebolo, R., Israelian, G., Filippenko, A.V. & Chornock, R. 2011, *ApJ*, 738, 95
- González Hernández, J.I., Rebolo, R. & Casares, J. 2012, *ApJ*, 744, L25
- Greenhill, J.G. et al. 2006, *MNRAS*, 372, 1129
- Grudzinska, M. et al. 2015, *MNRAS*, arXiv150403146
- Harlaftis, E.T., Marsh, T.R., Dhillon, V.S. & Charles, P.A. 1994, *MNRAS*, 267, 473
- Harlaftis, E.T., Horne, K. & Filippenko, A.V. 1996, *PASP*, 108, 762
- Harlaftis, E.T., Steeghs, D., Horne, K. & Filippenko, A.V. 1997, *AJ*, 114, 1170
- Hessman, F.V. 1988, *A&AS*, 72, 515
- Hessman, F.V., Robinson, E.L., Nather, R.E. & Zhang, E.-H. 1984, *ApJ*, 286, 747
- Horne, K., Wade, R.A. & Szkody, P. 1986, *MNRAS*, 219, 791
- Horne, K., Wood, J.H. & Stiening, R.F. 1991, *ApJ*, 378, 271
- Horne, K., Welsh, W.F. & Wade, R.A. 1993, *ApJ*, 410, 357
- Hynes, R.I. et al. 2002, *MNRAS*, 330, 1009
- Ioannou, Z., Robinson, E.L., Welsh, W.F. & Haswell, C.A. 2004, *AJ*, 127, 481
- Jonker, P.G. et al. 2011, *ApJS*, 194, 18
- Khargharia, J., Froning, C.S. & Robinson, E.L. 2010, *ApJ*, 716, 1105
- Khargharia, J., Froning, C.S., Robinson, E.L. & Gelino, D.M. 2013, *AJ*, 145, 21
- Kraft, R.P., Krzeminski, W. & Mumford, G.S. 1969, *ApJ*, 158, 589
- Kreidberg, L., Bailyn, C.D., Farr, W. & Kalogera, V. 2012, *ApJ*, 757, 36
- Lasota, J.-P. 2001, *NewAR*, 45, 449
- Littlefair, S.P. et al. 2008, *MNRAS*, 388, 1582
- Maccarone, T.J. 2005, *MNRAS*, 360, L30
- Maccarone, T.J. & Patruno, A. 2013, *MNRAS*, 428, 1335
- Marsh, T.R., Horne, K. & Shipman, H.L. 1987, *MNRAS*, 225, 551
- Marsh, T.R., Horne, K., Schlegel, E.M., Honeycutt, R.K. & Kaitchuck, R.H. 1990, *ApJ*, 364, 637
- Marsh, T.R., Robinson, E.L. & Wood, J.H. 1994, *MNRAS*, 266, 137
- Martín, E.L., Casares, J., Charles, P.A. & Rebolo, R. 1995, *A&A*, 303, 785
- Menou, K., Narayan, R. & Lasota, J.-P. 1999, *ApJ*, 513, 811
- Miller-Jones, J.C.A., Jonker, P.G., Maccarone, T.J., Nelemans, G., Calvelo, D. E. 2011, *ApJ*, 739, L18
- Morales-Rueda, L., Still, M.D., Roche, P., Wood, J.H. & Lockley, J.J. 2002, *MNRAS*, 329, 597
- Narayan, R. & McClintock, J.E. 2005, *ApJ*, 623, 1017
- Narayan, R. & McClintock, J.E. 2008, *NewAR*, 623, 1017
- Neustroev, V.V. & Zharikov, S. 2008, *MNRAS*, 386, 1366

- North, R.C., Marsh, T.R., Moran, C.K.J., Kolb, U., Smith, R.C. & Stehle, R. 2000, MNRAS, 337, 1215
- North, R.C., Marsh, T.R., Kolb, U., Dhillon, V.S. & Moran, C.K.J. 2002, MNRAS, 313, 383
- Orosz, J.A., Bailyn, C.D., Remillard, R.A., McClintock, J.E. & Foltz, C.B. 1994, ApJ, 436, 848
- Orosz, J.A. & Bailyn, C.D. 1995, ApJ, 446, L59
- Orosz, J.A., Bailyn, C.D., McClintock, J.E. & Remillard, R.A. 1996, ApJ, 468, 380
- Orosz, J.A. et al. 2002, ApJ, 568, 845
- Orosz, J.A., McClintock, J.E., Remillard, R.A. & Corbel, S. 2004, ApJ, 616, 376
- Orosz, J.A. et al. 2011, ApJ, 730, 75
- Özel, F., Psaltis, d., Narayan, R. & McClintock, J.E. 2010, ApJ, 725, 1918
- Patterson, J., Thorstensen, J.R. & Knigge, C. 2008, PASP, 120, 510
- Patterson, J., Richman, H., Kemp, J. & Mukai, K. 1998, PASP, 110, 403
- Peters, C.S. & Thorstensen, J.R. 2005, PASP, 117, 1386
- Pfahl, E., Rappaport, S. & Podsiadlowski, P. 2003, ApJ, 597, 1033
- Pyrzas, S. et al. 2012, PASP, 124, 204
- Remillard, R., Orosz, J.A., McClintock, J.E. & Bailyn, C.D. 1996, ApJ, 459, 226
- Ritter, H. & King, A.R. 2002, ASP, 261, 531
- Ritter, H. & Kolb, U. 2003, A&A, 404, 301
- Robinson, E.L. 1974, ApJ, 193, 191
- Rodríguez-Gil, P. et al. 2007, MNRAS, 377, 1747
- Rodríguez-Gil, P. et al. 2009, A&A, 496, 805
- Romani, R.W. 1998, A&A, 333, 583
- Savoury, C.D.J. et al. 2011, MNRAS, 415, 2025
- Savoury, C.D.J., Littlefair, S.P., Marsh, T.R., Dhillon, V.S., Parsons, S.G., Copperwheat, C.M. & Steeghs, D. 2012, MNRAS, 422, 469
- Shahbaz, T., Watson, C.A. & Dhillon, V.S. 2014, MNRAS, 440, 504
- Shafter, A.W. & Harkness, R.P. 1986, AJ, 92, 658
- Smak, J. 1984, Acta Astron., 34, 93
- Southworth, J. et al. 2006, MNRAS, 373, 687
- Southworth, J., Hickman, R.D.G., Marsh, T.R., Rebassa-Mansergas, A., Gänsicke, B.T., Copperwheat, C. M. & Rodríguez-Gil, P. 2009, A&A, 507, 929
- Skidmore, W., Mason, E., Howell, S.B., Ciardi, D.R., Littlefair, S. & Dhillon, V.S. 2000, MNRAS, 318, 429
- Steeghs, D., O'Brien, K., Horne, K., Gomer, R. & Oke, J.B. 2001, MNRAS, 323, 484
- Steeghs, D., Howell, S.B., Knigge, C., Gänsicke, B.T., Sion, E.M. & Welsh, W. 2007, ApJ, 667, 442
- Stover, R.J. 1981, ApJ, 249, 673
- Tanaka, Y. & Shibazaki, N. 1996, ARA&A, 34, 607
- Tappert, C., Thorstensen, J.R., Fenton, W.H., Bennert, N., Schmidtobreick, L. & Bianchini, A. 2001, A&A, 380, 533
- Thorstensen, J.R., Fenton, W.H., Patterson, J., Kemp, J., Halpern, J. & Baraffe, I. 2002a, PASP, 114, 1117
- Thorstensen, J.R., Fenton, W.H., Patterson, J., Kemp, J., Krajci, T. & Baraffe, I. 2002b, ApJ, 567, L49
- Thorstensen, J.R., Fenton, W.H. & Taylor, C.J. 2004, PASP, 116, 300
- Tomsick, J.A., Heindl, W.A., Chakrabarty, D., Halpern, J.P. & Kaaret, P. 2001, ApJ, 559, L123
- Torres, M.A.P., Casares, J., Martínez-Pais, I.G. & Charles, P.A. 2002, MNRAS, 334, 233

- Tulloch, S.M., Rodríguez-Gil, P. & Dhillon, V.S. 2009, MNRAS, 397, L82
- van den Heuvel, E.P.J. 1992, Proc. Inter. Space Year Conf. ESA ISY-3, p.29.
- Wade, R.A. & Horne, K. 1988, ApJ, 324, 411
- Warner, B. 1986, MNRAS, 222, 11
- Watson, C. A., Steeghs, D., Shahbaz, T. & Dhillon, V.S. 2007, MNRAS, 382, 1105
- Webb, N.A., Naylor, T., Ioannou, Z., Charles, P.A. & Shahbaz, T. 2000, MNRAS, 317, 528
- Wood, J., Horne, K., Berriman, G., Wade, R., O'Donoghue, D. & Warner, B. 1986, MNRAS, 219, 629
- Wood, J. & Horne, K. 1990, MNRAS, 242, 606
- Wood, M.A. et al. 2005, ApJ, 634, 570
- Yungelson, L.R., Lasota, J.-P., Nelemans, G., Dubus, G., van den Heuvel, E.P.J., Dewi, J. & Portegies Zwart, S. 2006, A&A, 454, 559
- Zurita, C. et al. 2000, MNRAS, 316, 137

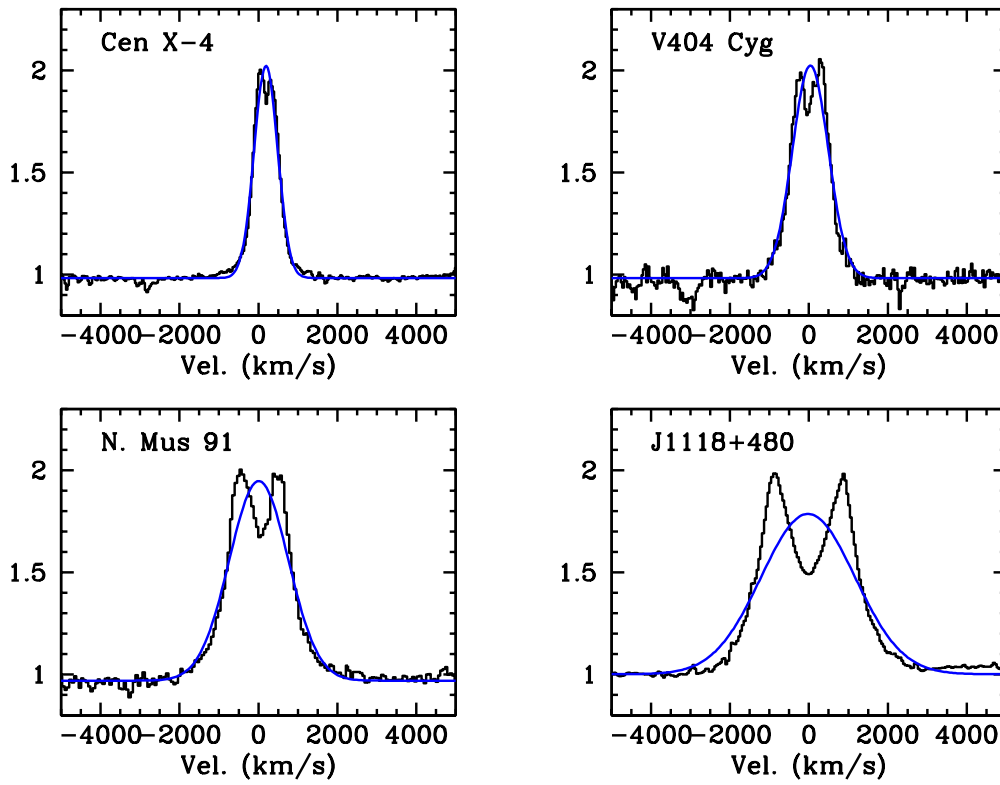


Fig. 1.— Example of Gaussian fits to H α profiles in SXTs. A selection of average spectra, representing the entire range of $FWHM$ s, is depicted.

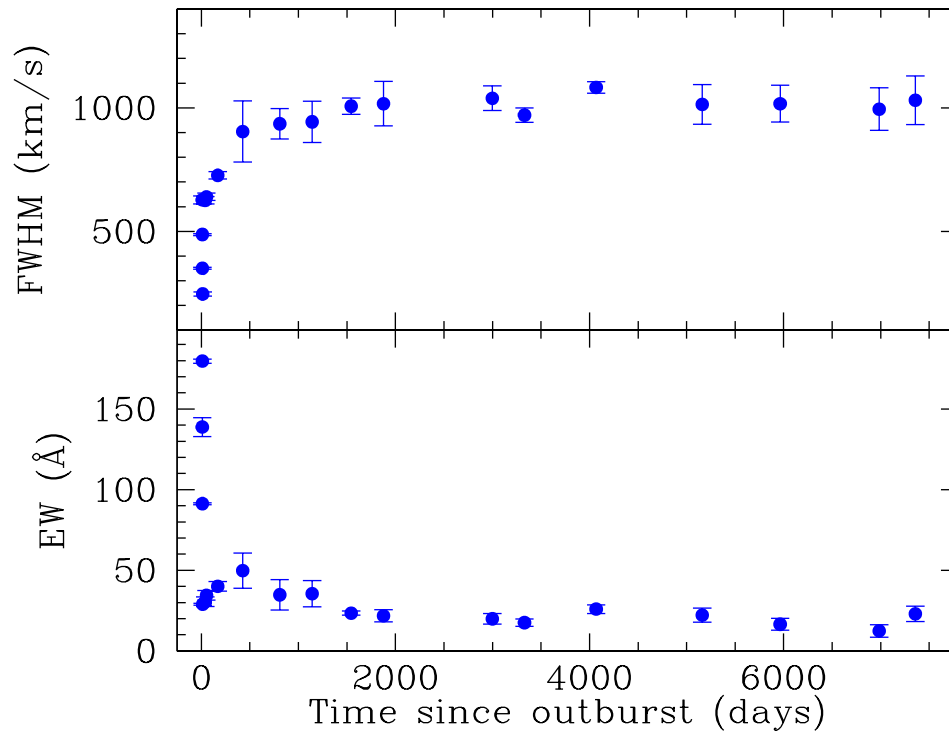


Fig. 2.— Long-term (20 year) evolution of the $FWHM$ and EW of the H_{α} line in V404 Cyg. Individual points have been co-added into 50 day bins except for the first 9 data points where 1-day bins were used. Errorbars reflect variability within the bin.

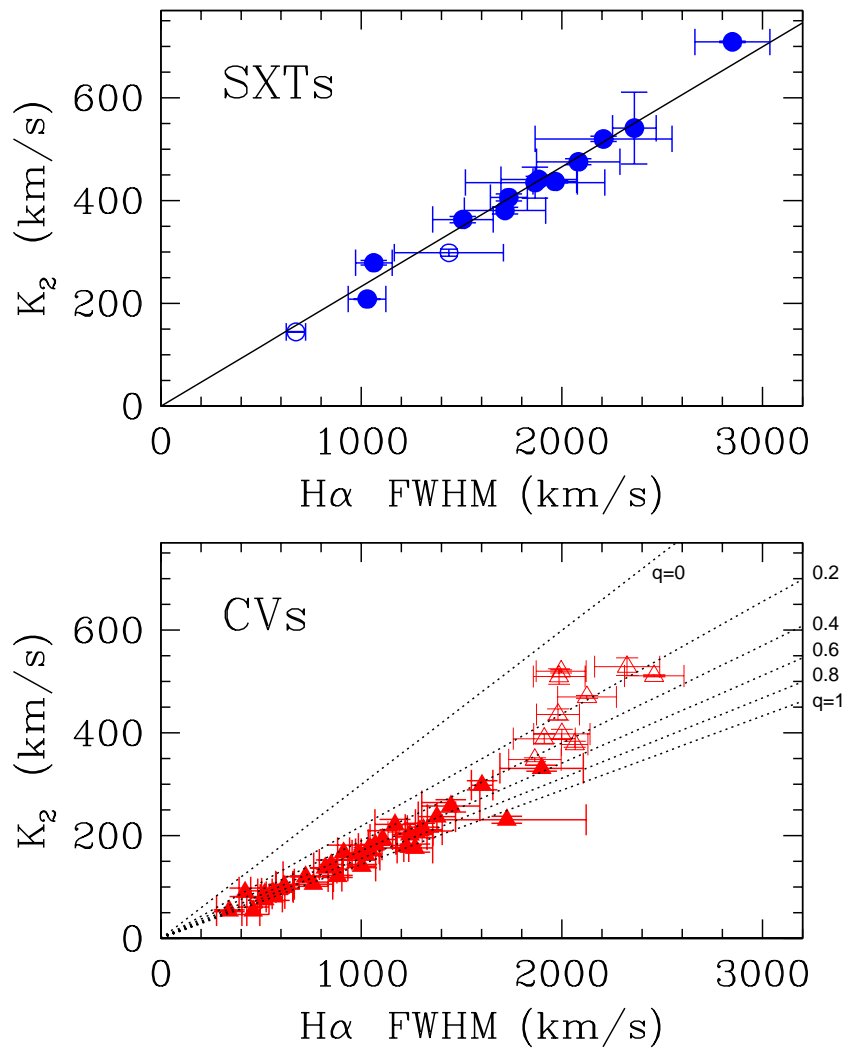


Fig. 3.— Top: the $FWHM - K_2$ correlation for SXTs with the best linear fit. Blue solid circles indicate BHs while Ns are marked by open circles. Bottom: the $FWHM - K_2$ correlation for CVs. Filled triangles indicate CVs above the period gap while open triangles those below/within the gap. Like in the case of SXTs, long period CVs display a tight $FWHM - K_2$ correlation although with a flatter slope. Dotted lines mark theoretical correlations from eq. 5-6 for $q = 0 - 1$ and $\alpha = 0.43$.

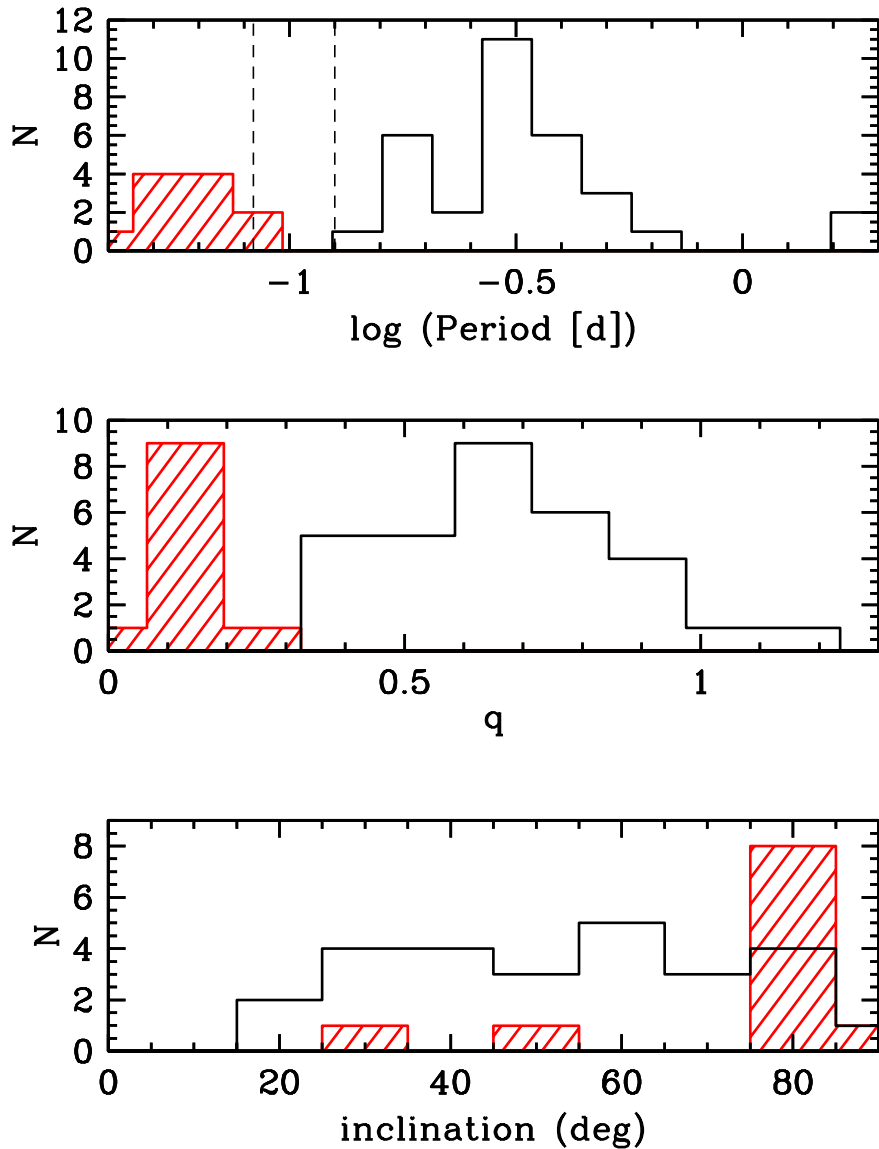


Fig. 4.— Distribution of orbital periods (top panel), mass ratios (middle) and inclinations (bottom) for the test sample of CVs. The white histogram represents CVs with orbital periods above the period gap while the red shaded histogram those below/within the gap. The period gap is indicated by dashed vertical lines in the top panel. All the CVs from the white histogram possess K_2 determinations based on radial velocity curves of the donor stars while those in the red shaded histogram on modeling eclipsing light curves. The only exceptions to the latter are the ultra-short period system EI Psc and the period gap CV SDSS J1300-3052. It can be seen that short period CVs have very low mass ratios and are strongly biased toward high inclinations (with the exception of the 2 CVs just mentioned).

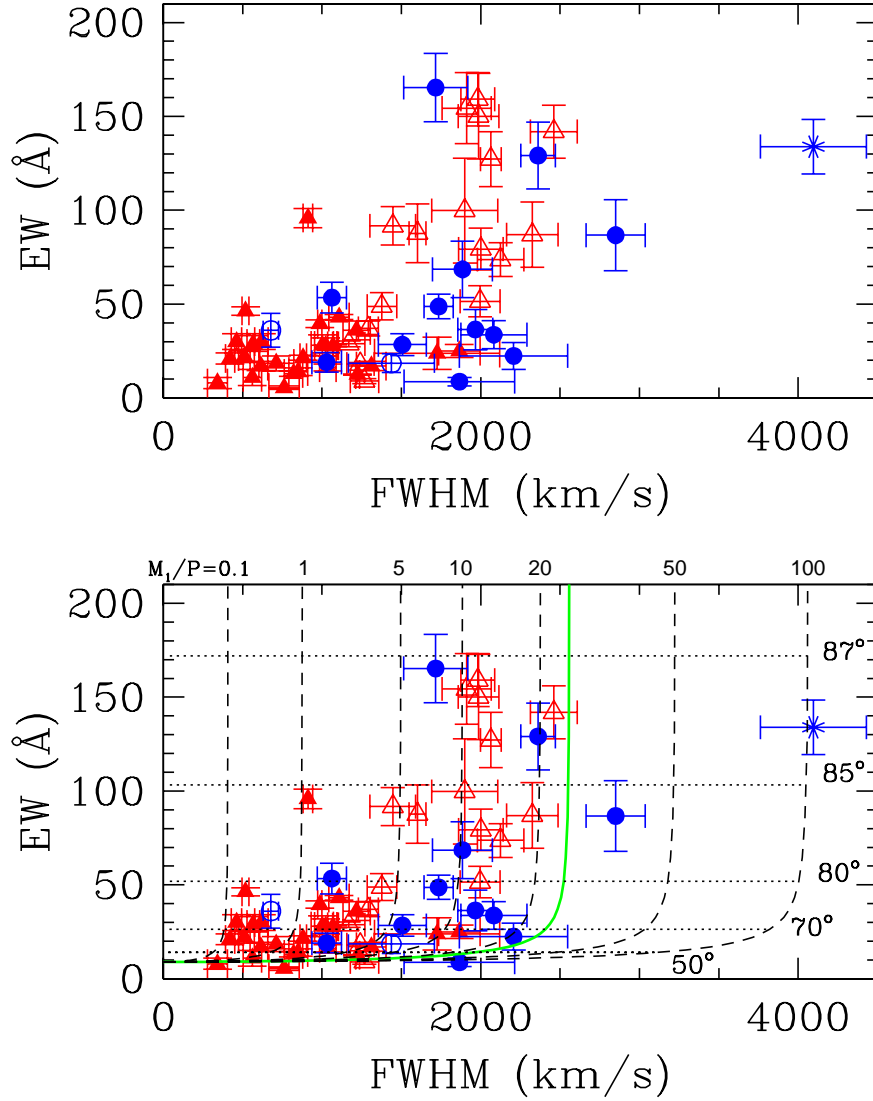


Fig. 5.— Top: SXTs and CVs in the $FWHM - EW$ plane. Same symbol code is used as in Fig. 3, except for open triangles which now indicate eclipsing CVs. Bottom panel: dashed vertical lines correspond to constant M_1/P_{orb} values (expressed in units of M_\odot/d) while horizontal dotted lines indicate various inclinations, in an idealized case where EW s are fortshortened by a factor $\cos i$ due to disc continuum visibility. The green solid line defines the maximum $FWHM$ predicted for CVs.

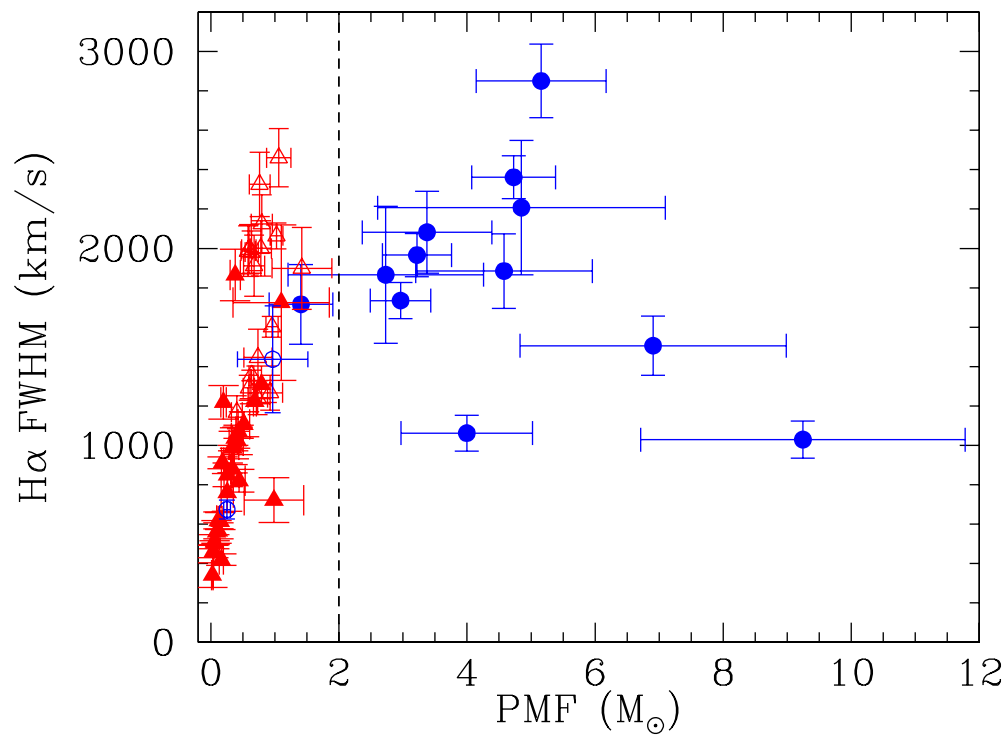


Fig. 6.— Preliminary mass functions obtained from K_2 values derived through the $FWHM - K_2$ correlation for SXTs. Same symbol code is used as in Fig. 5.

TABLE 1
DATABASE OF X-RAY TRANSIENTS

Object	# Spectra	Year	Resolution (km/s)	ref
Black Holes				
V404 Cyg	266	1989-2009	6-180	1-8
BW Cir	96	1995-2006	70-110	9-10
XTE J1550 -564	33	2001, 2008	55-165	11-12
N. Oph 77	1	1993	180	13
N, Mus 91	29	1993-1995	74-90	14
GS 2000+25	25	1995	196	15
A0620-00	20	2000	7	16
XTE J1650-500	15	2002	35	17
N Vel 93	1	1998	120	18
XTE J1859+226	10	2010	255	19
GRO J0422+320	21	1994-1995, 2009	230-630	8, 20
XTE J1118+480	120	2011	120	21
Neutron Stars				
Cen X-4	90	1993-2002	6-74	22-24
XTE J2123-058	20	2000	123-183	25

References. — (1) Casares et al. (1991); (2) Casares & Charles (1992a); (3) Casares et al. (1992b); (4) Casares et al. (1993); (5) Casares & Charles (1994); (6) Hynes et al. (2002); (7) González Hernández et al. (2011); (8) This paper; (9) Casares et al. (2004); (10) Casares et al. (2009a); (11) Orosz et al. (2011); (12) Orosz et al. (2002); (13) Remillard et al. (1996); (14) Casares et al. (1997); (15) Casares et al. (1995b); (16) González Hernández & Casares (2010); (17) Orosz et al. (2004); (18) Filippenko et al. (1999); (19) Corral-Santana et al. (2011); (20) Casares et al. (1995a); (21) González Hernández et al. (2012); (22) Torres et al. (2002); (23) D’Avanzo et al. (2005); (24) Casares et al. (2007); (25) Casares et al. (2002) .

TABLE 2
 DATABASE OF CATAclysmic VARIABLES.

Object	# Spectra	Year	Resolution (km/s)	ref
GK Per	8	1992, 1995, 1998	25-70	1-2
SDSS 2044-04	-	2001-2004	190-210	3
BV Cen	63	2004	10	4
RX 1951.7+3716	-	2001-2004	190-210	3
UY Pup	-	2002-2003	190-210	5
EY Cyg	103	1998-2001, 2004	15-20	6
DX And	4	1993	180	7
SY Cnc	28	1992, 1998-1999, 2003, 2008	25-70	1,8
AT Ara	-	2000	100	9
RU Peg	2	2008	60	2
GY Hya	-	2001-2004	190-210	3
CH UMa	16	2008-2009	60-320	2
V392 Hya	-	2001-2004	190-210	3
RY Ser	-	2003	190-210	5
HS 0218+3229	56	2002	55-75	10
EM Cyg	3	2008	60	2
Z Cam	12	2009	60	2
SDSS 0813+45	-	2002	190-210	5
V426 Oph	4	2006	40	2
SS Cyg	23	2008	60-250	2
LY UMa	-	2000	190-500	11
BF Eri	5	2009	235	2
TT Crt	-	2000-2003	190-210	5
AH Her	10	1980-1981	60	12
EX Dra	31	2001	50	2
HS 2325+8205	42	2005, 2007	215	13
DQ Her	4	2009	60	2
SDSS J100658.40+233724	68	2008	140	14
SS Aur	28	2008, 2013	90-320	2
U Gem	32	1999, 2008	16-320	2,15
CN Ori	17	1986	137	16
IP Peg	28	1988, 2009	50-150	2,17
CTCV J1300-3052	24	2010	45	18
QZ Ser	-	2002	200	19
Z Cha	-	1984	150	20
HT Cas	10	2008	60-190	2
OY Car	28	2010	46	21
V2051 Oph	31	1998, 2009	55-430	2,23
SDSS 103533.02+055158.3	51	2006	70	23
WZ Sge	384	1996	25	24
SDSS J143317.78+101123.3	38	2008	32	25

TABLE 2—*Continued*

Object	# Spectra	Year	Resolution (km/s)	ref
SDSS 1507+52	-	2006	160	26
EI Psc = J2329+0628	-	2001	180	27

NOTE.—Information on SDSS 2044-04, RX 1951.7+3716, UY Pup, AT Ara, GY Hya, V392 Hya, RY Ser, SDSS 0813+45, LY UMa, TT Crt, CN Ori, QZ Ser, Z Cha, SDSS 1507+52 and EI Psc has been extracted from literature. In the case of CN Ori, the *FWHM* and *EW* values are obtained from 17 individual measurements listed in table 1 of Barrera & Vogt (1989). The AH Her spectra are phased binned averages.

References. — (1) Martín et al. (1995); (2) this paper; (3) Peters & Thorstensen (2005); (4) Watson et al. (2007); (5) Thorstensen et al. (2004); (6) Echevarría et al. (2007); (7) Bruch et al. (1997); (8) Casares et al. (2009b); (9) Bruch (2003); (10) Rodríguez-Gil et al. (2009); (11) Tappert et al. (2001); (12) Horne et al. (1986); (13) Pyrzas et al. (2012); (14) Southworth et al. (2009); (15) Echevarría et al. (2007); (16) Barrera & Vogt (1989); (17) Harlaftis et al. (1994); (18) Savoury et al. (2012); (19) Thorstensen et al. (2002a); (20) Marsh et al. (1987); (21) Copperwheat et al. (2012); (22) Steeghs et al. (2001); (23) Southworth et al. (2006); (24) Skidmore et al. (2000), (25) Tulloch et al. (2009); (26) Patterson et al. (2008); (27) Thorstensen et al. (2002b) .

TABLE 3
X-RAY TRANSIENTS

Object	P (d)	K_2 (km/s)	$FWHM$ (km/s)	EW (Å)	M_1 (M_\odot)	i (deg)	ref [†]
Black Holes							
V404 Cyg	6.47129	208.4 ± 0.6	1029 ± 94	19.0 ± 5.2	$9.0^{+0.2}_{-0.6}$	67^{+3}_{-1}	1,2
BW Cir	2.54451	279.0 ± 4.7	1062 ± 91	53.4 ± 8.2			3
XTE J1550-564	1.5420333	363.1 ± 6.0	1506 ± 151	28.4 ± 5.8	11.5 ± 3.9	75 ± 4	4
N. Oph 77	0.5228	441.0 ± 6.0	1885 ± 189	68.5 ± 15.1	6.2 ± 1.2	70 ± 10	5
N. Mus 91	0.4326058	406.0 ± 7.0	1735 ± 92	48.7 ± 6.5	7.0 ± 0.6	54 ± 2	6,7
GS 2000+25	0.3440915	519.9 ± 5.1	2207 ± 341	22.4 ± 7.2	$5.5-8.8$	$58-74$	8,9
A0620-00	0.32301405	437.1 ± 2.0	1966 ± 110	36.4 ± 10.8	6.6 ± 0.3	51 ± 1	10,11
XTE J1650-500	0.3205	435.0 ± 30.0	1866 ± 348	8.7 ± 2.3			12
N Vel 93	0.285206	475.4 ± 5.9	2082 ± 208	33.7 ± 7.4			13
XTE J1859+226	0.274	541.0 ± 70.0	2361 ± 109	129.1 ± 17.8			14
GRO J0422+320	0.2121600	380.6 ± 6.5	1716 ± 202	165.3 ± 18.2			15
XTE J1118+480	0.1699337	708.8 ± 1.4	2850 ± 187	86.7 ± 18.9	$6.9-8.2$	$68-79$	16,17
Neutron Stars							
Cen X-4	0.6290522	144.6 ± 0.3	678 ± 48	36 ± 9	$1.94^{+0.37}_{-0.85}$	32^{+8}_{-2}	18,19
XTE J2123-058	0.24821	298.5 ± 6.9	1437 ± 272	18.5 ± 5.0	1.5 ± 0.3	73 ± 4	20,21

[†] This column provides references for the adopted values of P , K_2 , M_1 and i .

References. — (1) Casares (1996); (2) Khargharia et al. (2010); (3) Casares et al. (2009a); (4) Orosz et al. (2011); (5) Harlaftis et al. (1997); (6) Orosz et al. (1996); (7) Gelino et al. (2001); (8) Harlaftis et al. (1996); (9) Ioannou et al. (2004); (10) González Hernández & Casares (2010); (11) Cantrell et al. (2010); (12) Orosz et al. (2004); (13) Filippenko et al. (1999); (14) Corral-Santana et al. (2011); (15) Webb et al. (2000); (16) González Hernández et al. (2012); (17) Khargharia et al. (2013); (18) Casares et al. (2007); (19) Shahbaz et al. (2014); (20) Tomsick et al. (2001); (21) Zurita et al. (2000).

TABLE 4
CATAclysmic VARIABLES

Object	P (d)	K_2 (km/s)	$FWHM$ (km/s)	EW (\AA)	ref [†]
GK Per	1.9968	120.5± 0.7	722 ± 113	18.1± 4.0	1
SDSS 2044-04	1.68	90.0± 8.0	420 ± 29	21.0 ± 2.9	2
BV Cen	0.611179	137.3± 0.3	820 ± 58	13.0 ± 1.4	3-4
RX 1951.7+3716	0.492	81.0 ± 7.0	566 ± 40	29.0 ± 4.1	2
UY Pup	0.479269	102.0± 4.0	615 ± 43	17.0 ± 2.4	5
EY Cyg	0.4593249	54.0± 2.0	341 ± 63	8.0 ± 3.0	5
DX And	0.4405019	105.8± 3.8	761 ± 96	5.4 ± 0.9	7-8
SY Cnc	0.3823753	88.0± 2.9	560 ± 58	10.9 ± 4.2	9
AT Ara	0.37551	99.5± 3.2	618 ± 43	30.0 ± 4.2	10
RU Peg	0.3746	121.0± 2.0	881 ± 21	21.4 ± 01.4	11
GY Hya	0.3472309	176.0±8.0	1267± 89	9.0 ± 1.3	2
CH UMa	0.3431843	76.0± 3.0	518 ± 22	46.3 ± 2.2	5
V392 Hya	0.324952	144.0± 9.0	850± 60	14.0 ± 2.0	2
RY Ser	0.3009	87.0± 6.0	519 ± 36	22.0 ± 3.1	5
HS 0218+3229	0.297229661	162.4± 1.4	1023 ± 70	27.9 ± 4.0	12
EM Cyg	0.290909	202.0± 3.0	1242 ± 86	18.0 ± 0.9	13-14
Z Cam	0.289840	193.0± 17.0	1107 ± 64	43.1 ± 1.3	15
SDSS 0813+45	0.2890	54.0± 7.0	461 ± 32	30.0 ± 4.2	5
V426 Oph	0.285314	179.0± 2.0	1224 ± 13	12.5 ± 0.3	16-17
SS Cyg	0.27512973	165.0± 1.0	986 ± 14	39.5 ± 2.0	17-18
LY UMa	0.271278	141.0± 3.0	1002 ± 70	28.0 ± 5.6	19
BF Eri	0.270881	182.5± 0.9	1069 ± 34	27.7 ± 0.5	20
TT Crt	0.2683522	212.0± 5.0	1310 ± 92	17.0 ± 2.4	5
AH Her	0.258116	175.0± 2.0	1037 ± 52	16.2 ± 1.9	18,21
EX Dra	0.20993698	210.0± 14.0	1292 ± 63	37.0 ± 4.0	22-23
HS 2325+8205	0.194334535	237.0± 28.0	1377 ± 93	48.8 ± 7.2	24
DQ Her	0.193620919	227.0± 10.0	1168 ± 101	28.8 ± 1.5	25-26
SDSS J100658+233724	0.18591324	258.0± 12.0	1446 ± 144	91.7 ± 10.2	27
SS Aur	0.1828	167.0± 15.0	911 ± 30	95.8 ± 5.2	28-29
U Gem	0.17690619	298.4 ± 9.0	1602 ± 53	87.7 ± 15.6	30-31
CN Ori	0.16319006	231.0± 7.0	1725 ± 395	23.8 ± 8.6	31-32
IP Peg	0.1582061029	331.3± 5.8	1899 ± 208	99.8 ± 28.0	33-34
CTCV J1300-3052	0.088940717	378.0± 6.0	2064 ± 66	127.2 ± 14.7	35-36
QZ Ser	0.0831612	207.0± 5.0	1218 ± 85	36.0 ± 5.0	37
Z Cha	0.0744992335	398.0± 9.0	2000 ± 140	79.3 ± 11.1	38-39
HT Cas	0.0736472029	389.0± 9.0	1912 ± 155	154.4 ± 18.9	40-41
OY Car	0.0631209343	470.0± 2.7	2125 ± 147	73.7 ± 9.0	42-43
V2051 Oph	0.0624278634	436.0± 11.0	1981 ± 107	159.1 ± 14.2	44-45
SDSS 103533.02+055158.3	0.0570067	520.0±3.0	1996 ± 125	51.5 ± 8.3	46
WZ Sge	0.056688	510.0± 15.0	1986 ± 129	150.1 ± 22.8	47-48
SDSS J143317.78+101123.3	0.054240679	511.0±2.0	2460 ±148	141.9±14.1	46

TABLE 4—*Continued*

Object	P (d)	K_2 (km/s)	$FWHM$ (km/s)	EW (Å)	ref [†]
SDSS 1507+52	0.04625834	529.0±17.0	2325 ±163	87.0±17.4	49
EI Psc = J2329+0628	0.044566	348.0± 4.0	1865 ± 131	25.0 ± 3.5	50

[†] This column provides references for the adopted values of P and K_2 .

References. — (1) Morales-Rueda et al. (2002); (2) Peters & Thorstensen (2005); (3) Gilliland (1982); (4) Watson et al. (2007); (5) Thorstensen et al. (2004); (6) Echevarría et al. (2007); (7) Bruch et al. (1997); (8) Drew et al. (1993); (9) Casares et al. (2009b); (10) Bruch (2003); (11) Stover (1981); (12) Rodríguez-Gil et al. (2009); (13) Robinson (1974); (14) North et al. (2000); (15) Kraft et al. (1969); (16) Hessman (1988); (17) North et al. (2002); (18) Hessman et al. (1984); (19) Tappert et al. (2001); (20) Neustroev & Zharikov (2008); (21) Horne et al. (1986); (22) Baptista et al. (2000); (23) Billington et al. (1996); (24) Pyrzas et al. (2012); (25) Wood et al. (2005); (26) Horne et al. (1993); (27) Southworth et al. (2009); (28) Shafter & Harkness (1986); (29) Davey & Smith (1992); (30) Marsh et al. (1990); (31) Friend et al. (1990); (32) Barrera & Vogt (1989); (33) Copperwheat et al. (2010); (34) Beekman et al. (2000); (35) Savoury et al. (2011); (36) Savoury et al. (2012); (37) Thorstensen et al. (2002a); (38) Wood et al. (1986); (39) Wood & Horne (1990); (40) Borges et al. (2008); (41) Horne et al. (1991); (42) Greenhill et al. (2006); (43) Copperwheat et al. (2012); (44) Baptista et al. (2003); (45) Baptista et al. (1998); (46) Littlefair et al. (2008); (47) Patterson et al. (1998); (48) Steeghs et al. (2007); (49) Patterson et al. (2008); (50) Thorstensen et al. (2002b).